JOURNAL OF GEOPHYSICAL RESEARCH, VOL. 94, NO. B7, PAGES 9341-9352, JULY 10, 1989

On the Source of Cross-Grain Lineations in the Central Pacific Gravity Field

DAVID C. MCADOO

National Geodetic Survey, Charting and Geodetic Services, National Ocean Service, NOAA, Rockville, Maryland

DAVID T. SANDWELL

Center for Space Research, University of Texas at Austin

Subtle lineations in the marine gravity field of the central Pacific derived from Seasat altimeter data were observed by Haxby and Weissel (1986). They suggested that these "cross-grain" lineations were evidence of small-scale convection beneath the Pacific plate. We have examined these features by comparing multiple, collinear gravity and bathymetry profiles in the Fourier transform domain. Our nine gravity profiles were each obtained by stacking (averaging) three or more individual, repeat Geosat/ERM altimeter passes. Prior to stacking, the individual Geosat passes were fit to a cubic spline and then differentiated along track to produce along-track deflections of the vertical (or horizontal gravity). Corresponding bathymetric profiles were produced by projecting, onto Geosat ground tracks, bathymetric observations from six R/V *Thomas Washington* legs and three R/V *Conrad* legs that virtually coincide with these Geosat tracks. After Fourier transforming the resulting gravity and bathymetry profiles, we estimate admittances of gravity to bathymetry. These admittances are generally low; they also tend to be negative at very short wavelengths ($\lambda < 50$ km). They are consistent with models of flexural isostatic compensation by a very thin lithosphere (approximately 2 km). They are not consistent with models of dynamic compensation. We suggest, therefore, that either (1) these cross-grain lineations began to form very near the East Pacific Rise or (2) they formed on older, anomalously weak lithosphere. We also suggest that the gravity lineations result primarily from loads beneath the seafloor in combination with, secondarily, loads on the seafloor. Depths of these subseafloor loads appear not to exceed significantly typical Moho depths.

INTRODUCTION

Direct observations of sea surface topography (which approximates the geoid) by microwave satellite altimeters such as Seasat and Geosat provide a vast amount of exciting new information about the marine gravity field across the globe. For example, we cite the subtle gravity lineations or "cross-grain" patterns which were discovered in Seasat data from the central Pacific by *Haxby and Weissel* [1986]. These lineations (Figure 1) are oriented roughly parallel to the direction of absolute Pacific plate motion, are separated from one another by one hundred to several hundred kilometers, and have typical amplitudes of roughly 10 mGal. In fact, these lineations will be the focus of this paper.

That these lineations had previously escaped detection by conventional measurements of gravity and bathymetry is not at all surprising. Both Seasat and Geosat are sensitive detectors of all but the shortest-wavelength ($\lambda < 25$ km) signals in the marine gravity field (Geosat is, as we shall see, a more sensitive detector than Seasat).

Neither these lineations nor any other features which might be discovered using satellite altimeter data can, by themselves, be inverted to yield a reasonably unique model of crustal and/or mantle source structures. However, when these altimeter observations are analyzed in combination with comparable bathymetric observations, such models of source structure can be developed. This is exactly what we have done. Following procedures quite similar to those of *McKenzie and Bowin* [1976], we have Fourier transformed (1) sequences of along-track, Geosat gravity observations and (2) coincident sequences of bathymetry. Then the relationships, or admittances, that are observed between these Fourier transforms of gravity and bathymetry can be compared with those predicted by various models of compensation, both isostatic and dynamic.

We have not been able to model exactly the source(s) and compensating mechanisms which give rise to these lineations. We have, however, determined, in general, what constitutes a reasonable model, i.e., where the source masses are located and how they are compensated. Recall that *Haxby and Weissel* [1986] proposed that the lineations were a result of small-scale mantle convection of the sort described originally by *Richter and Parsons* [1975]. Their proposition was based largely on Seasat observations alone because suitably collinear tracks of bathymetry or seismic reflection profiles were not then available. We now find that dynamic compensation models, or models wherein the lineations result directly from small-scale convection in the upper mantle, do not agree with our combined gravity and bathymetry observations. *Buck and Parmentier* [1986] have suggested that these gravity lineations were produced when the seafloor was very young and that they were subsequently "frozen in" (see also *Lin and Parmentier* [1985]). This suggestion remains a possibility. However, our study includes crust ranging in age from a very young 6 Ma to a mature 75 Ma; nowhere within this range do we find admittances suggestive of dynamic compensation. In fact, observed admittances vary only slightly over this age range.

What then does constitute a reasonable model? According to our results, a model in which the source loads occur on or within the crust and are compensated at relatively shallow depths. *Winterer and Sandwell* [1987] have suggested that the cross grain may have resulted from tensional deforma-

Paper number 89JB00614.
0148-0227/89/89JB-00614$05.00

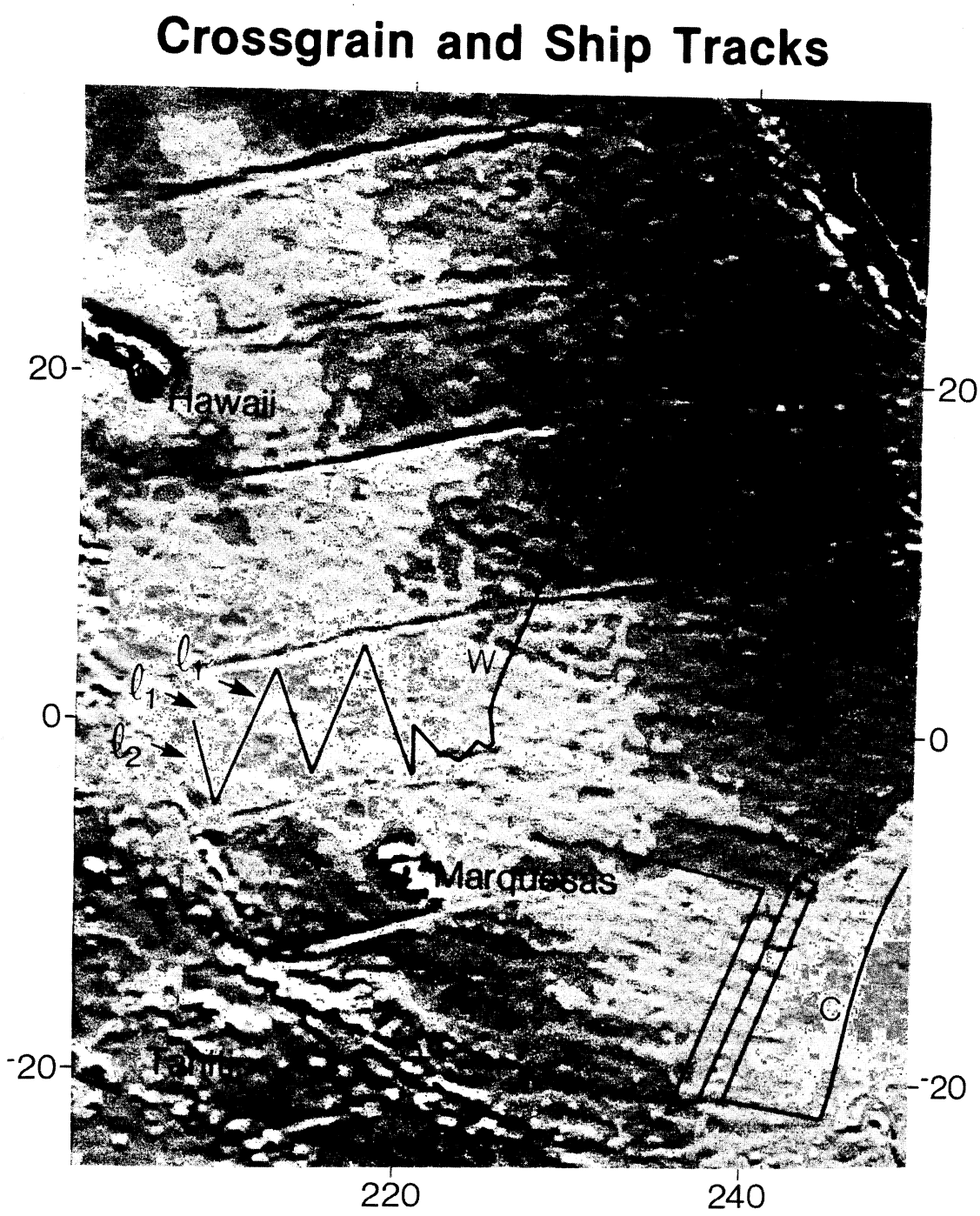

Fig. 1. Gravity field of the central Pacific Ocean from Seasat due to *Haxby* [1987]. Shiptracks of the R/V *Thomas Washington* (marked W) and the R/V *Robert Conrad* (marked C) are shown. Three cross-grain lineations are labeled l_1, l_1', and l_2. (Original in color.)

tion or stretching of the lithosphere. They observed, using Sea Beam and seismic reflection profiling, that narrow, volcanic ridges are associated with the cross grain, and they suggested that these ridges result from magmatic filling of tensional cracks in the lithosphere. This tensional cracking and filling could have loaded the lithosphere with intracrustal, intrusive bodies. Such loading would be consistent with our observed admittances.

The intent of this paper is to introduce significant constraints on models of formation of the cross grain. The ultimate model should await the final processing and analysis of all available shipboard data. For example, admittance models developed in this paper could be further tested using shipboard gravity collected from the R/V *Thomas Washington*. However, these data presently contain considerable navigation errors. The R/V *Robert Conrad* shipboard gravity data are not available. Also, backstripping of sediments, a complex task, should help considerably in modeling shiptrack segments (e.g., zigs 4 and 5) where thick sediments render bathymetry and gravity incoherent.

Data Analysis

Bathymetry

The bathymetric data were all collected by the Sea Beam multibeam sonar systems on board the R/V *Thomas Washington* in February and March 1987 and the R/V *Robert Conrad* in June–August 1985.

As can be seen in Figures 1 and 2*a*, the R/V *Washington* shiptrack includes six, relatively straight segments or "zigs." Three of these zigs (2, 4, and 6) are nearly collinear with descending, Geosat/ERM ground tracks (shown as dashed lines in Figure 2). The other three zigs (zags?) (1, 3, and 5) are nearly collinear with ascending Geosat ground tracks. The longest zig (6) extends roughly 3000 km from 1°N to 24°N and includes substantial bathymetric signals associated with the Clarion Fracture Zone. To better isolate the cross-grain signal, we will use zig 6′, a shortened version of zig 6, which extends only to 16°N. Five of these segments or zigs (1–5) are comparably short, from 6° to 9° in length. These five are all contained between the Clipperton and Galapagos fracture zones (see Figure 1) and hence each overlies crust of nearly constant age. All six R/V *Washington* zigs overlie crust of moderate age (40–75 Ma).

The R/V *Conrad* ship tracks (see Figures 1 and 2*b*) include three 1500-km-long "legs" which are also nearly collinear with Geosat ground tracks. These three legs (A, B, and C) overlie young oceanic crust (age 6–20 Ma). They are closely spaced (~150 km) and thereby provide redundant observations of the lineations. This redundancy allows us to estimate admittances with increased confidence.

The bathymetric data are projected onto the nearby Geosat ground tracks; they are then interpolated along-track using a Gaussian filter with a half width of 1.7 km to obtain predicted ocean depths at Geosat observation points. The resulting bathymetric profiles are shown in Figures 3*a*–11*a*. Along zigs 6, 1, 2, and 3 (Figures 3*a*, 4*a*, 5*a*, and 6*a*) as well as legs A, B, and C (Figures 9*a*, 10*a*, and 11*a*), bathymetric swells can be seen which clearly correlate with the geoidal expression of the cross-grain lineations (see Figures 3*b*, 4*b*, 5*b*, 6*b*, 9*b*, 10*b*, and 11*b*). However, along zigs 4 and 5 (Figures 7*a* and 8*a*) one can see little or no bathymetric evidence of the cross grain. This region is covered with pelagic sediments which may obscure such evidence along these two zigs.

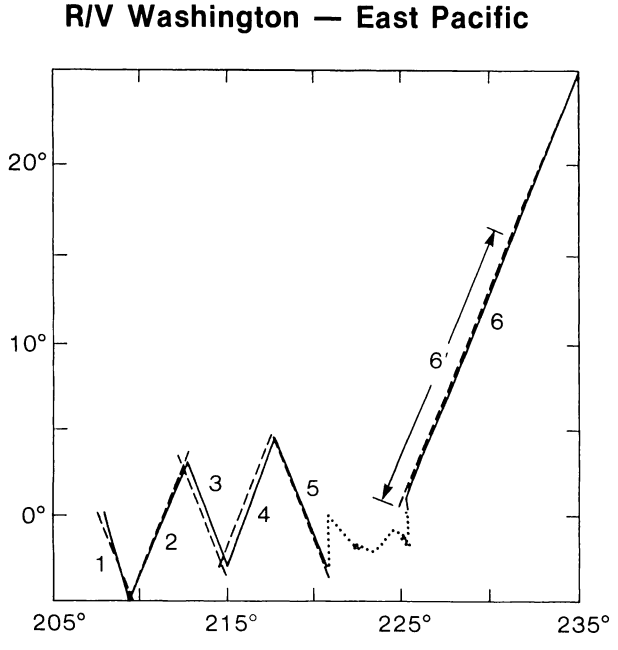

Fig. 2*a*. Ship track zigs and zags, numbered 1–6, of the R/V *Thomas Washington*. Dashed lines are nearby Geosat/ERM ground track segments. Zig 6′ is a shortened version of zig 6.

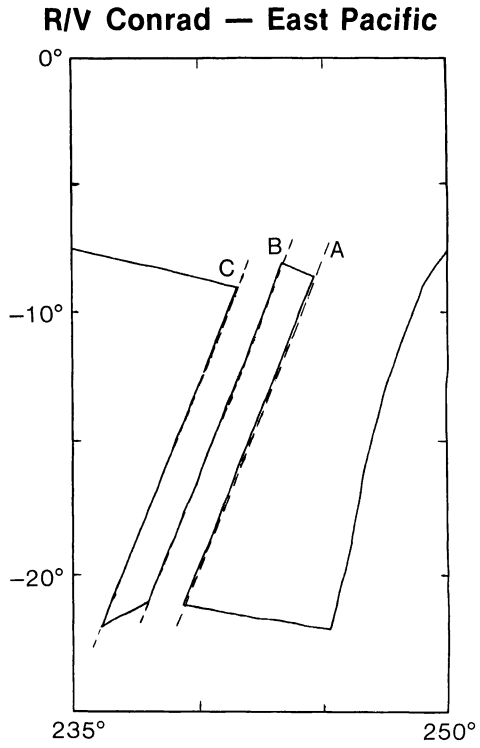

Fig. 2*b*. Ship track "legs," A, B, and C, of the R/V *Robert Conrad*. Nearby Geosat ground tracks are dashed.

Marine Geoid and Gravity From Geosat

The Geosat microwave radar altimeter, which was launched by the U.S. Navy in March 1985 and remains operational today, makes precise, direct observations of sea surface topography in a manner quite similar to that of its predecessor, Seasat. Geosat is, however, a quieter altimeter than Seasat. Furthermore, in its unclassified Exact Repeat Mission (ERM) it reobserves the same ground track every 17.05 days permitting us to stack or average repeat passes and eliminate time-varying oceanographic effects from the sea surface observations. Hence we obtain from Geosat a more precise estimate of the marine geoid or gravity field particularly at wavelengths of several hundred kilometers where mesoscale oceanographic effects are at a maximum. In this study we have averaged passes from three or more ERM cycles to obtain our individual profiles of marine geoid and gravity.

Our techniques for analyzing the Geosat data are very similar to those described by *Sandwell and McAdoo* [1988]. Geosat data from Geophysical Data Records [*Cheney et al.*, 1987] were edited when the rms about the 1-s mean exceeded 10 cm. Data were compressed from 10 points per second to 2 per second by averaging over 0.5-s intervals. Cubic splines were then fitted to the along-track data; the splines were used to interpolate along-track and to reregister the data at

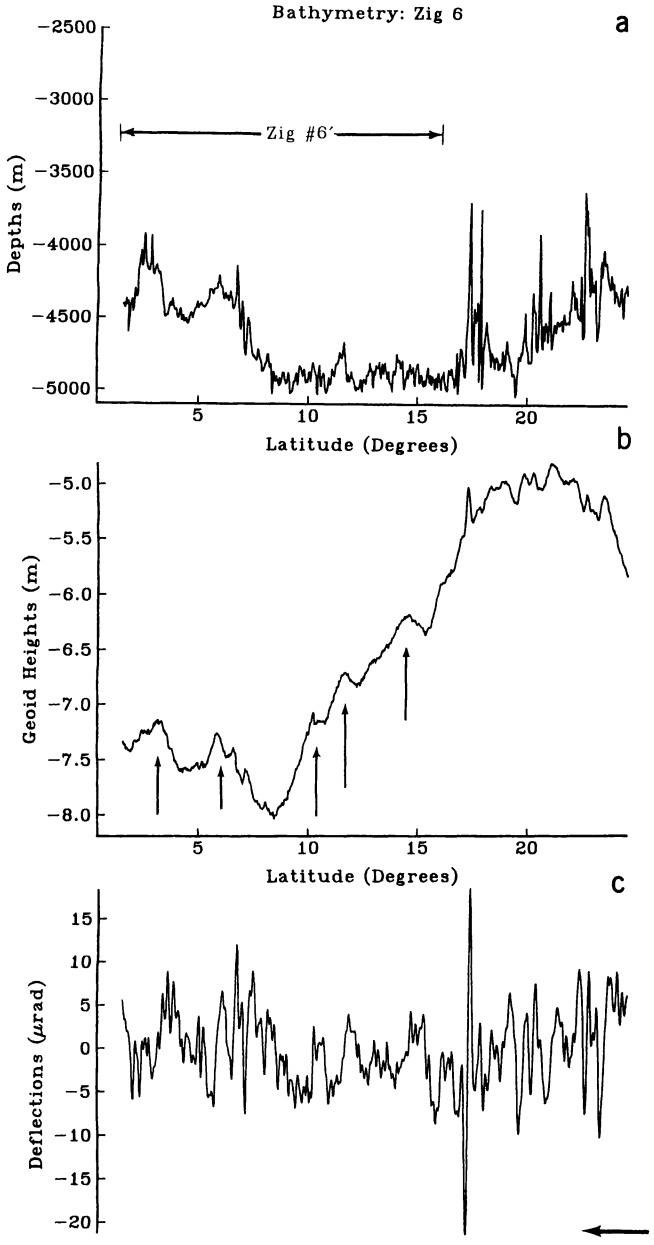

Fig. 3. (*a*) Bathymetry from zig 6 projected onto nearby ERM ground track. (*b*) Geoid height profile along zig 6. From a stack of seven Geosat/ERM passes. Degree 8, GEM L-2 background geoid removed. Crests of cross-grain lineation are marked with arrows. (*c*) Deflections of the vertical along zig 6. Deflections are positive in satellite direction. From a stack of seven Geosat/ERM passes. Degree 8, GEM L-2 background geoid removed.

standardized points separated by a fixed interval of 0.03° arc length. Along-track slopes were then computed at these points by evaluating the derivative of the cubic splines. These along-track slopes are, in the absence of oceanographic effects, equivalent to deflections of the vertical and are proportional to horizontal gravity disturbances (1 μrad of slope yields roughly 1 mGal of horizontal gravity). Individual collinear passes of heights and slopes could then be averaged together. Finally, we high pass filtered the geoid and gravity profiles (Figures 3*b*–11*b* and 3*c*) by subtracting a degree-and-order-8, GEM L-2 background field from both heights and slopes. Wavelengths contained in this degree-and-order-8 background field are long (>5000 km), much longer than those associated with the cross-grain lineations. Removal of this field will therefore produce negligible cutoff effects or Gibbs phenomenon at the relatively short wavelengths of interest.

To construct the geoid and deflection profiles for zig 6 (see Figures 3*b* and 3*c*), Geosat descending passes from days 70, 87, 104, 121, 138, 155, and 172 of 1987 were used. Similarly, for zig 1 (see Figure 4*b*) ascending passes from days 35, 52, and 69 of 1987 were used; for zig 2 (Figure 5*b*) descending passes from days 145 and 162 of 1987 as well as day 322 of 1986 were used; and for zig 3 (Figure 6*b*) ascending passes from days 30, 47, and 64 of 1987 were used. Because so little cross-grain signal is evident in the bathymetry along zigs 4 and 5 (see Figures 7*a* and 8*a*), we did not bother stacking repeat Geosat passes along these two zigs. We did, however, derive geoid height profiles (high-pass filtered) from single Geosat passes: for zig 4 (Figure 7*b*) we used a descending pass from day 86 of 1987 and for zig 5 (Figure 8*b*) we used an ascending pass from day 322 of 1986. To construct the geoid and deflection profiles for *Conrad* leg A (see Figure 9*b*), we used descending Geosat passes from days 16, 33, and 50 of 1987. For leg B (Figure 10*b*), we used descending passes from days 30, 47, and 64 of 1987, and for leg C (Figure 11*b*), we used passes from days 44, 61, and 78.

In all of the geoid height profiles (Figures 3*b*–11*b*) undulations associated with the cross-grain can be seen quite clearly. Most are marked with arrows. Note, in Figure 1, the

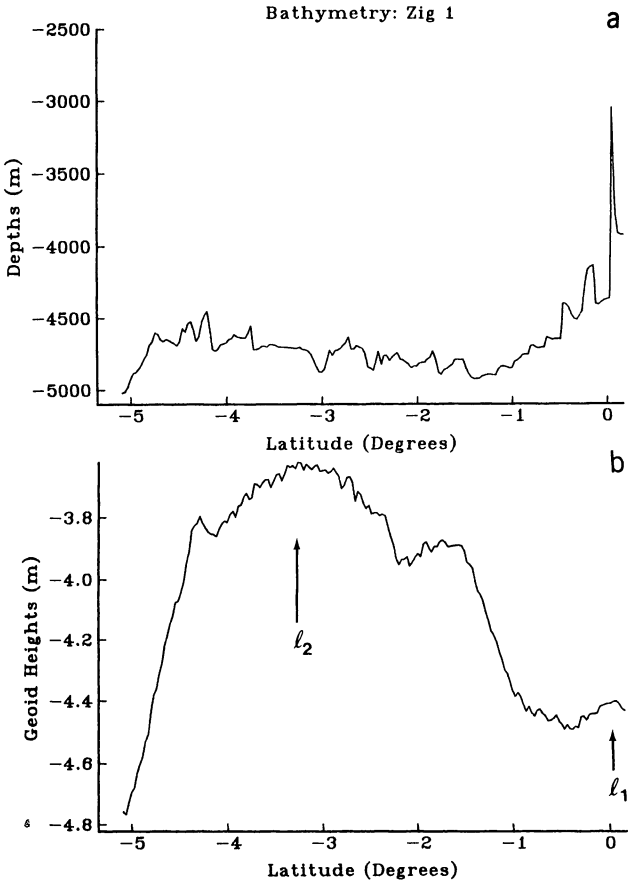

Fig. 4. (*a*) Bathymetry from zig 1. (*b*) Geoid height profile along zig 1 from stack of three passes. See Figure 3 caption.

three lineations labeled l_1, $l_{1'}$, and l_2. These three are also marked and labeled on the geoid profiles in Figures 4*b*–8*b*. These undulations have amplitudes of a few decimeters to 1 m and wavelengths of 150 km to several hundred kilometers. In Figures 9*b*, 10*b*, and 11*b*, a set of eight, regularly spaced, persistent lineations are marked. These eight trend perpendicularly to legs A, B, and C. Power spectra of the three geoid profiles (Figures 9*b*, 10*b*, and 11*b*) reveal a strong peak at a wavelength of 150 km. There are, of course, many geoid undulations in these profiles which are unrelated to the cross-grain phenomenon. Note, for example, in Figure 3*b* (zig 6), that the Clipperton and Clarion fracture zones produce significant geoidal signals at 6°N and 17°N, respectively. Also note that the Clarion fracture zone is excluded from zig 6′, the shortened version of zig 6.

The horizontal gravity or deflection-of-the-vertical profiles (see Figure 3*c*) contain essentially the same information that exists in the corresponding geoid profiles (see Figure 3*b*). One can not readily see the cross-grain signal in these deflection profiles simply because the deflection signal contains more high-frequency information than, and is out of phase with, the geoid signal. Therefore we have shown only one deflection profile, Figure 3*c*. We will, nonetheless, use these very same deflection profiles to estimate admittances in the section that follows. In principle, using deflections is equivalent to using geoid undulations. In practice, however, by using deflections we optimally high-pass filter and prewhiten the geoid profiles.

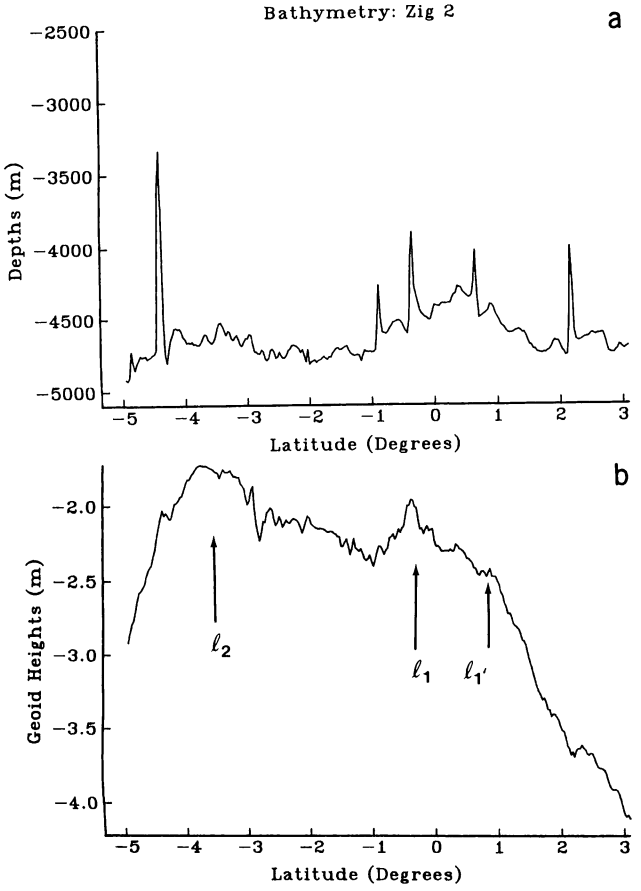

Fig. 5. (*a*) Bathymetry from zig 2. (*b*) Geoid height profile along zig 2 from stack of three passes. See Figure 3 caption.

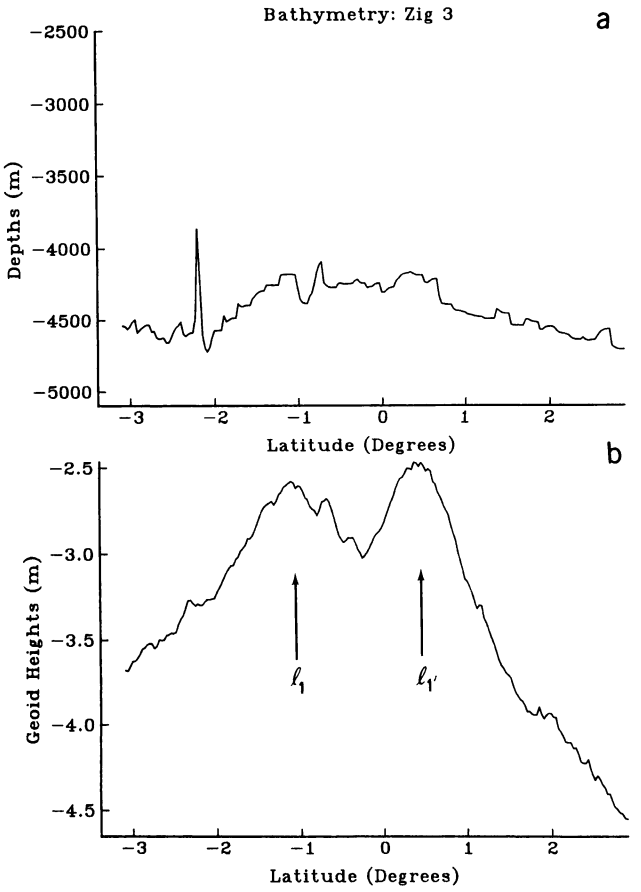

Fig. 6. (*a*) Bathymetry from zig 3. (*b*) Geoid height profile along zig 3 from stack of three passes. See Figure 3 caption.

Estimated Admittances Between Gravity and Bathymetry

McKenzie and Bowin [1976] showed (see also *Dorman and Lewis* [1970]) that in studies of relationships between gravity and bathymetry, results are more easily extracted by comparing these two signals in the discrete Fourier transform domain than in the spatial domain. We assume, as they did, that linear system theory applies. Therefore, in the spatial domain, an impulse response function $h(n)$ exists such that the convolution of bathymetry $b(n)$ with $h(n)$ yields gravity $g(n)$, i.e.,

$$g(n) = h(n) * b(n) \tag{1}$$

It is, however, the Fourier transform domain in which we choose to work. Therefore, we take the discrete Fourier transform of (1) and obtain 2

$$G(k) = Z(k)B(k) \tag{2}$$

where $G(k)$ and $B(k)$ are the discrete Fourier transforms of gravity and bathymetry, k is wave number defined by $k = 2\pi/\lambda$, and $Z(k)$ is the admittance or transfer function. Note that the convolution operation in (1) reduces simply to multiplication in (2). In the absence of noise we would simply use (2) to estimate admittance, i.e., $Z(k) = G(k)/B(k)$. In practice, however, we use an estimator recommended by *McKenzie and Bowin* [1976], specifically,

$$Z(k) = C(k)/E_b(k) \tag{3}$$

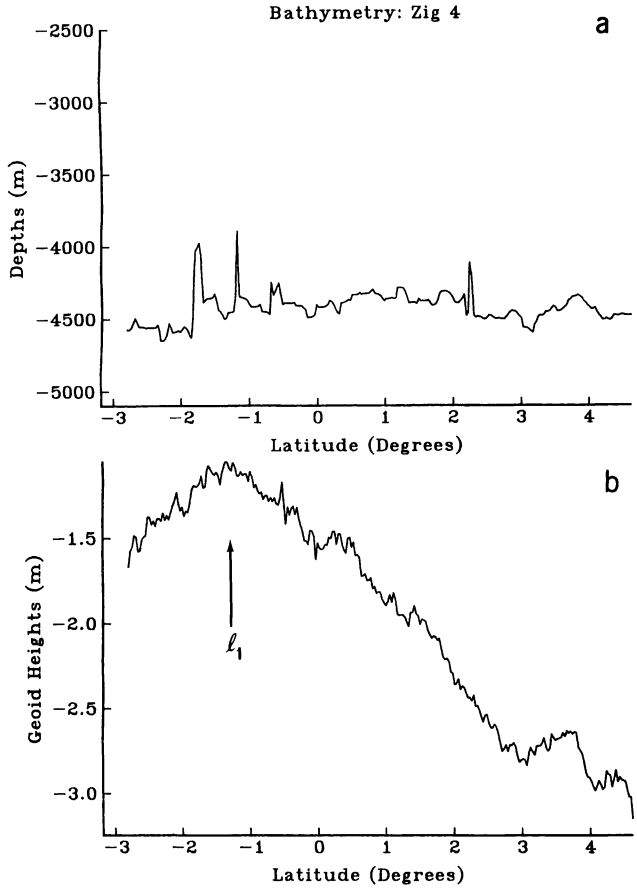

Fig. 7. (*a*) Bathymetry from zig 4. (*b*) Geoid height profile along zig 4 from one pass. See Figure 3 caption.

which is not biased by noise. In (3), $C(k)$ is the complex cross spectrum of gravity and bathymetry and $E_b(k)$ is the auto power spectrum of bathymetry. Admittances derived from observations using (3) can be compared directly with theoretical admittances which characterize various models of isostatic and dynamic compensation. In order to test the significance of these observed admittances we should check whether coherences differ appreciably from zero. We use *McKenzie and Bowin*'s [1976] definition of coherence γ^2, which is

$$\gamma^2(k) = C \cdot \bar{C}/E_b E_g \tag{4}$$

where overbar denotes complex conjugate and E_g is the auto power spectrum of gravity.

In order to compute auto spectra E_b and E_g, as well as the complex cross spectrum C, we use standard fast Fourier transform (FFT) techniques. We segment the bathymetry and gravity (deflection of vertical) sequences into, typically, eight parts. Lengths of individual input data sequences, before segmentation or padding with zeroes, range from about 200 points (zig 1) to more than 800 points (zig 6). The data segments are then windowed (Parzen). Spectra are derived for each segment. These segment spectra are, in turn, averaged to obtain ensemble, auto, and cross-spectral estimates. Inasmuch as legs A, B, and C represent somewhat redundant coverage, we combined the three, sequentially, into a single 1344-point gravity data sequence and a comparable bathymetric sequence. After segmentation into 21 parts and windowing, we obtained ensemble admittances. To assure that segmentation was not producing spurious admittances, we computed independent auto and cross spectra for the unsegmented sequences and then smoothed in wave number domain. Results were in good agreement.

Using (3) and the techniques described above, we have estimated complex admittances between horizontal gravity and bathymetry along each of six zigs as well as complex admittances for the combination of legs A, B, and C. The imaginary components of these estimated admittances are plotted in Figures 12*a*–12*f* for zig 6, zig 6′, zig 1, zig 2, and zig 3 and the combination of legs A, B, and C. Only imaginary components are plotted because theoretical admittances from compensation models (see below) are all strictly imaginary. That model admittances are imaginary reflects the 90° phase lag between theoretical gravity (horizontal) and bathymetry (see below). Associated phases are plotted in Figures 13*a*–13*f*. Deviations from the model-predicted phase of $\pm\pi/2$ rad are indicators of misfits to the model(s).

Note that admittances were not plotted for zigs 4 and 5. The coherences that we recovered between gravity and bathymetry along these two zigs were generally near zero; hence recovered admittances are of questionable significance here. Recall our earlier suggestion that sediments obscure the bathymetric signal along these two zigs. Coherences recovered for zig 1, the shortest of the lot, were also low; therefore admittances in Figure 12*c* should be viewed somewhat skeptically. Along zigs 2, 3, and 6 and legs A, B, and C, estimated coherences were appreciable; they were of

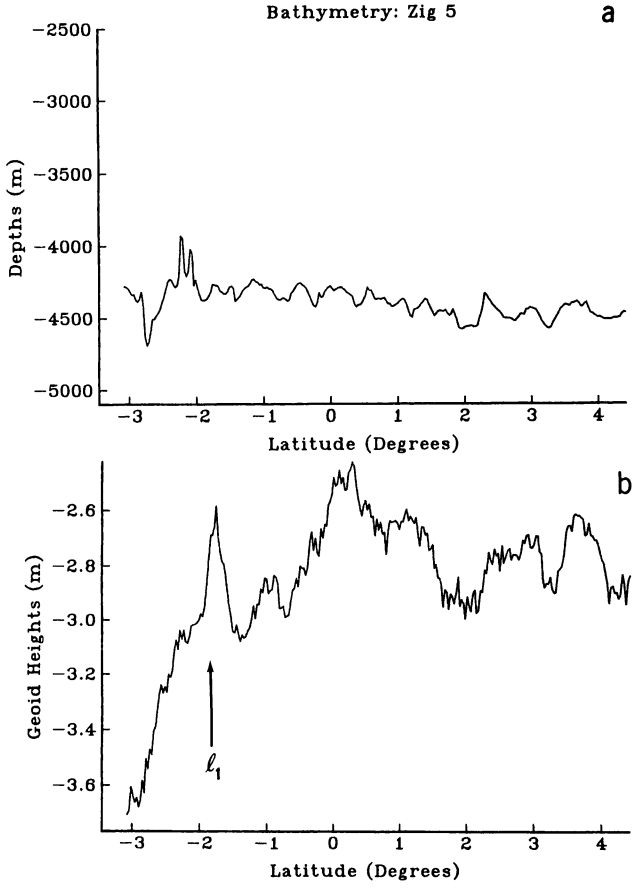

Fig. 8. (*a*) Bathymetry from zig 5. (*b*) Geoid height profile along zig 5 from one pass. See Figure 3 caption.

order 0.5. Generally, coherences were low, i.e., less than 0.3, at wavelengths of 100 km to several hundred kilometers; they were highest (0.5–0.8) in the waveband from 40 to 75 km. These coherences are reflected in the relative size of error bars in Figures 12*a*–12*e*: a smaller error bar results from a larger coherence. Specifically, the standard, sampling errors σ' of estimated admittances are computed from coherences using $\sigma' = Z[(\gamma^{-2} - 1)/2p]^{1/2}$, where p is the number of segments in the data sequence. This expression for standard error is from *Munk and Cartwright* [1966]; see *Watts* [1978] for an example application of this expression to analyses of gravity and bathymetry data.

Models

Loading on the Seafloor

We wish to compare the admittances which we have recovered from the observations with admittances that are predicted by models of isostatic compensation. We will test two models; both of which are flexural (or regional) compensation models. We will also test the two models in combination. In these models, loads are supported by flexural strength of an elastic lithosphere which is, in turn, buoyed by hydrostatic restoring forces from the fluid-like, underlying asthenosphere [*Barrell*, 1914; *Vening Meinesz*, 1939; *Gunn*, 1943].

The first of these two models is the very familiar, top loaded model (Figure 14*a*) in which loads are emplaced on the seafloor. The theoretical admittance or isostatic response function, as it is often called, is given by *McKenzie and Bowin* [1976], *Banks et al.* [1977], *Walcott* [1976], and elsewhere. The isostatic response function derived by these workers is that of vertical gravity to bathymetry (or topography). Let us denote this isostatic response function as $Z_g(k)$. The response function that we seek, however, is not $Z_g(k)$ but $Z_d(k)$, which is the response of deflections of the vertical (or horizontal gravity) to bathymetry. Inasmuch as we already have an expression for $Z_g(k)$ we can easily obtain the expression for $Z_d(k)$ with the following Hilbert transformation:

$$Z_d(k) = Z_g(k) \cdot i \cdot \text{sgn}\,(k)/g \tag{5}$$

where i is the imaginary unit, g is the acceleration of gravity, and sgn $(k) = 1$ when $k > 0$ and -1 when $k < 0$ [*Chapman*, 1979]. The resulting expression for the flexural response (or admittance) $Z_d(k)$ of top loaded lithosphere is

$$Z_d(k) = \frac{2\pi i \cdot \text{sgn}(k) G(\rho_c - \rho_w)}{g} e^{-kd} \cdot \left\{1 - \frac{e^{-kt}}{[1 + Dk^4/((\rho_m - \rho_c)g)]}\right\} \tag{6}$$

where d is ocean depth, t is crustal thickness, ρ_c is crustal density, ρ_w is seawater density, ρ_m is mantle density, and D is flexural rigidity. Flexural rigidity is given by $D = E T_e^3/[12(1 - \nu^2)]$, where T_e is the effective elastic thickness of

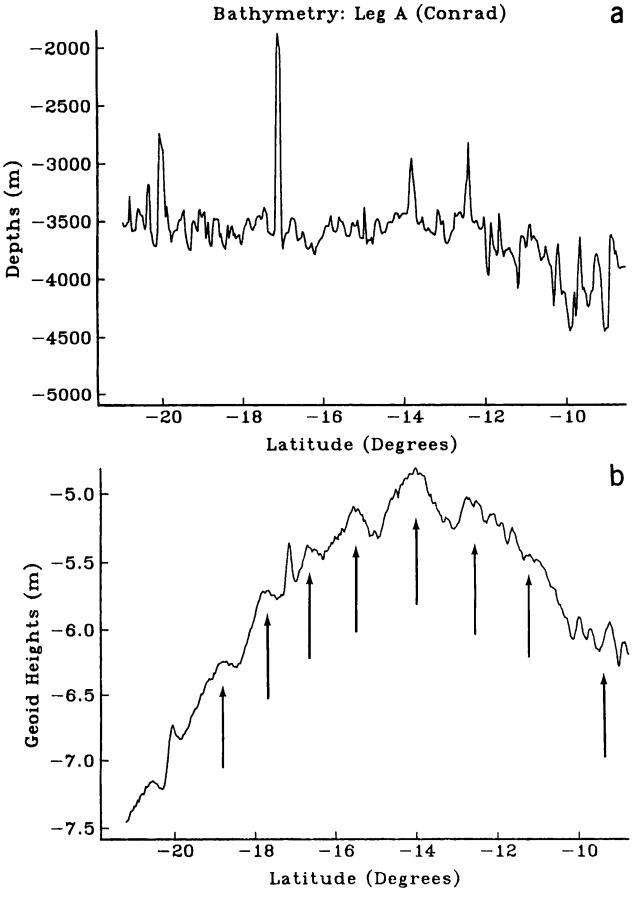

Fig. 9. (*a*) Bathymetry from *Conrad* leg A. Projected. (*b*) Geoid height profile along leg A from stack of three passes. See Figure 3 caption.

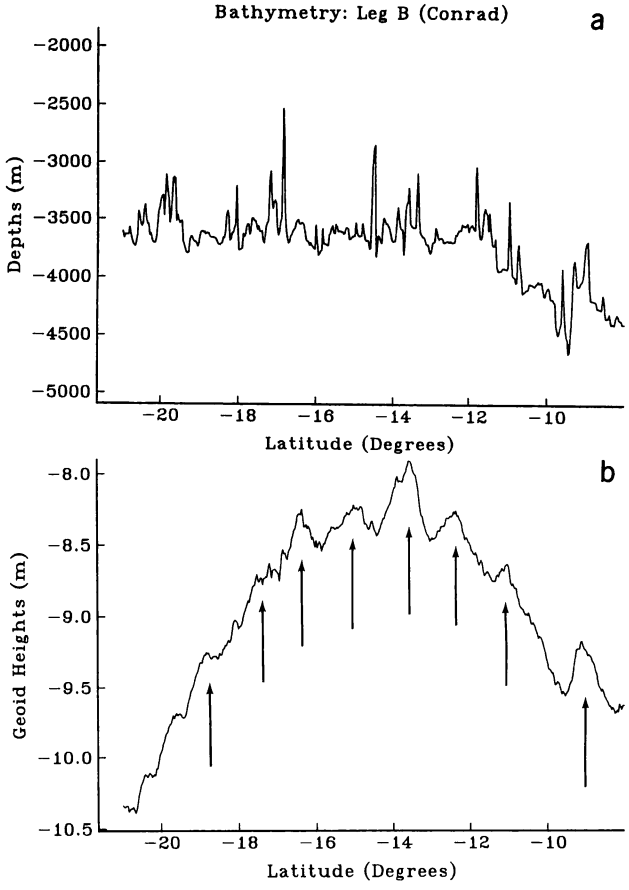

Fig. 10. (*a*) Bathymetry from *Conrad* leg B. Projected. (*b*) Geoid height profile along leg B from stack of three passes. See Figure 3 caption.

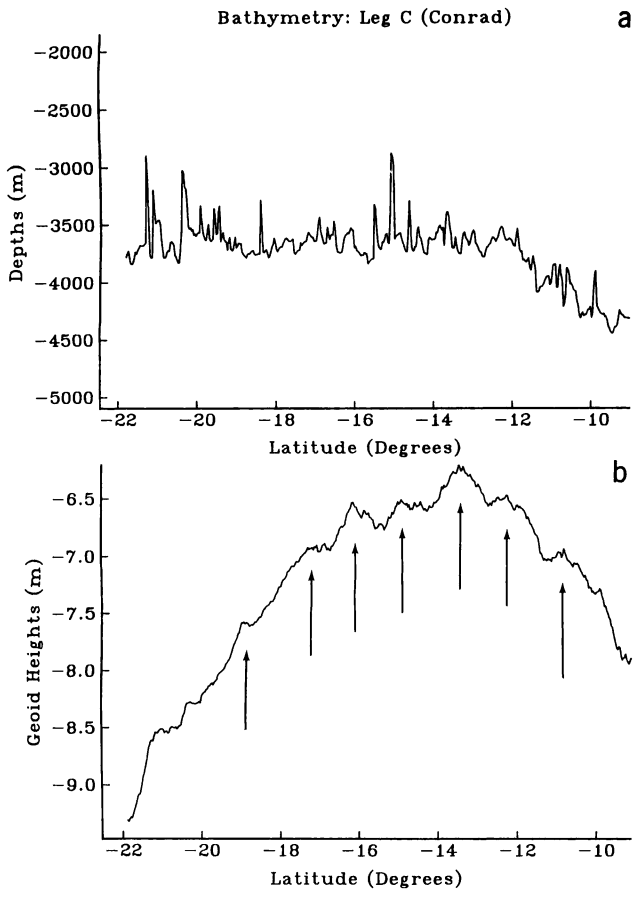

Fig. 11. (*a*) Bathymetry from *Conrad* leg C. Projected. (*b*) Geoid height profile along leg C from stack of three passes. See Figure 3 caption.

the lithosphere, ν is Poisson's ratio, and E is Young's modulus. Note that k is a scalar and that according to our model, topography and gravity vary in only one dimension. Equation (6) was used to generate theoretical admittances which are plotted as dashed lines in Figure 12*a*. In evaluating (6) we used $E = 7.0 \times 10^{10}$ N m^{-2}, $\nu = 0.25$, $\rho_m = 3.33 \times 10^3$ kg m^{-3}, $\rho_c = 2.8 \times 10^3$ kg m^{-3}, $\rho_w = 1.0 \times 10^3$ kg m^{-3}, $d = 5$ km, $t = 6$ km, and values for T_c of 2, 5, 10, and 25 km.

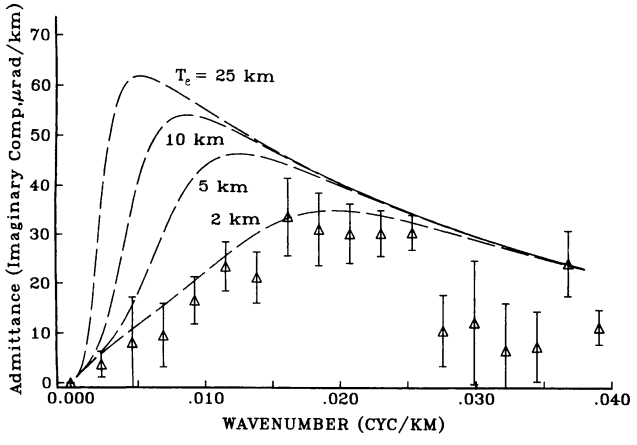

Fig. 12*a*. Admittances (imaginary component) observed along zig 6. Dashed lines are imaginary theoretical admittances predicted by a compensation model in which loads on the seafloor are supported by an elastic lithosphere of thickness T_c = 2, 5, 10, and 25 km.

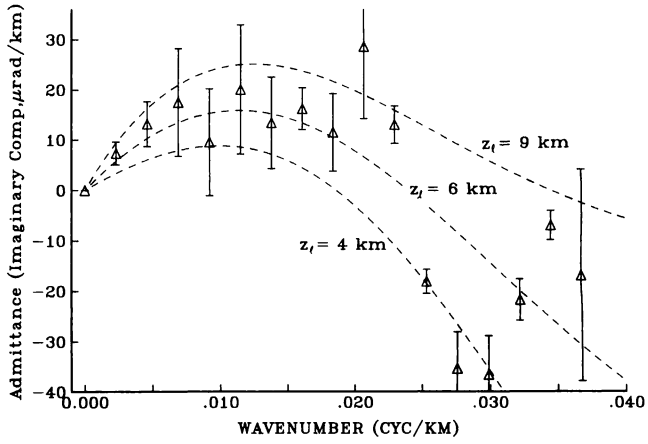

Fig. 12*b*. Admittances (imaginary component) observed along zig 6′. Dashed lines are imaginary admittances predicted by a compensation model in which loads at depths Z_l = 4, 6, and 9 km beneath the seafloor are supported by an elastic lithosphere of thickness 2 km.

Note in Figure 12*a* that the admittances derived from observations along zig 6 agree reasonably well with admittances (dashed lines) predicted by models wherein a thin lithosphere (2–5 km) is top loaded. Also note in Figure 13*a* that phases observed along this zig agree fairly well with the phase $\pi/2$ predicted by this same top-loaded model. One should not assume, however, that there exist no other models which satisfactorily describe admittances observed here. In fact, the model of a thin lithosphere loaded from beneath the seafloor (see below) will also describe, fairly well, these observed admittances. Note also that the 3000-km-long zig 6 includes much topography, particularly at the northern end (16°–24°N), which is apparently unrelated to the cross-grain lineations.

Loading Beneath the Seafloor

The second model of isostatic compensation which we test is quite similar to the first. In this model, also, loads are supported flexurally by a lithosphere which floats on a fluidlike asthenosphere. However, these loads are no longer emplaced on the seafloor but are assumed to be concentrated at some depth z_l beneath the seafloor (see Figure 14*b*). These

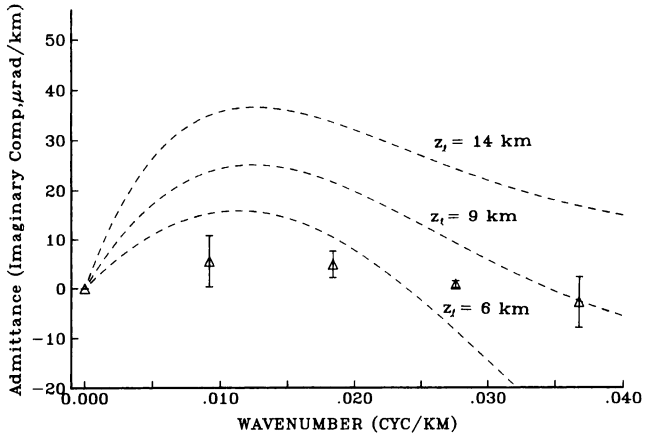

Fig. 12*c*. Admittances (imaginary component) observed along zig 1. Dashed lines are imaginary theoretical admittances predicted by a compensation model in which loads at depths, z_l = 6, 9, and 14 km beneath the seafloor are supported by an elastic lithosphere of thickness 2 km.

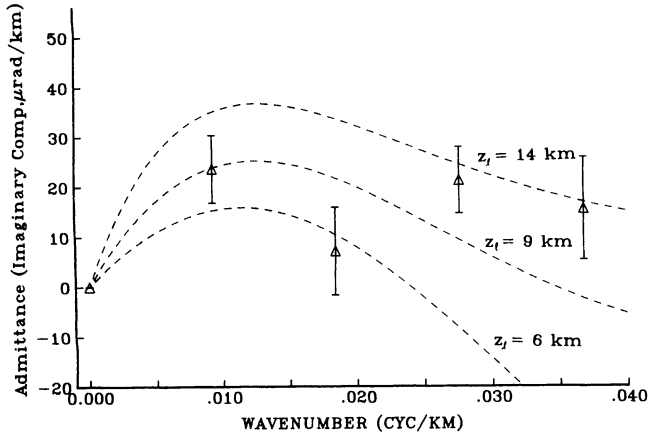

Fig. 12*d*. Admittances (imaginary component) observed along zig 2. Dashed lines are same as in Figure 12*c*.

loads can be thought of as relatively flat-lying bodies with a fixed density contrast $\delta\rho$ with respect to the surrounding country rock and a variable thickness $t_l(x)$. This model is essentially the same as that used by *McNutt* [1983] and *Forsyth* [1985] to describe isostatic compensation on continents. In order to obtain the expression for isostatic response (or admittance) which we require, we adapt their theoretical admittance to include the effects of an ocean layer and to describe the response of deflections of the vertical instead of vertical gravity (see equation (5), above). Note that before we use equation (5) we must first convert their admittances to describe the response of free-air gravity rather than Bouguer. After these adaptations we obtain the following expression for admittance:

$$Z_d(k) = \frac{2\pi i \cdot \text{sgn}\,(k) G(\rho_c - \rho_w)}{g} e^{-kd}\left\{1 + \frac{(\rho_m - \rho_c)}{(\rho_c - \rho_w)} e^{-kt} - \frac{(\rho_m - \rho_w)}{(\rho_c - \rho_w)}\left[1 + \frac{Dk^4}{(\rho_m - \rho_w)g}\right] e^{-kz_l}\right\} \quad (7)$$

Equation (7) was used to compute the theoretical admittances shown in Figures 12*b*, 12*c*, 12*d*, and 12*e*. In evaluating (7) we use same values for parameters E, ν, ρ_m, ρ_c, ρ_w, d, and t which were employed in evaluating (6), above.

Theoretical admittances which are plotted as dashed lines in Figure 12*b* represent a 2-km-thick lithosphere loaded at depths

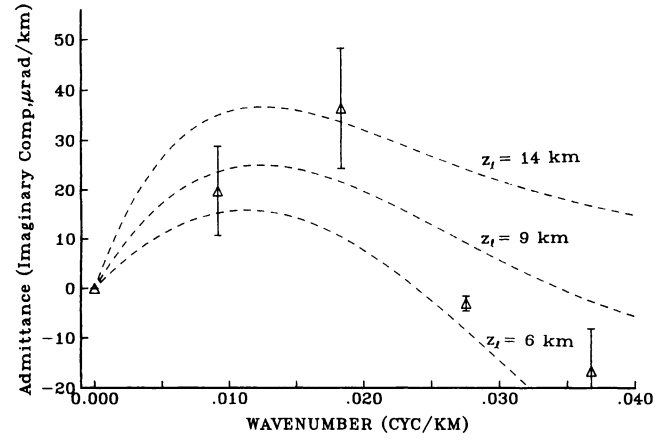

Fig. 12*e*. Admittances (imaginary component) observed along zig 3. Dashed lines are same as in Figure 12*c*.

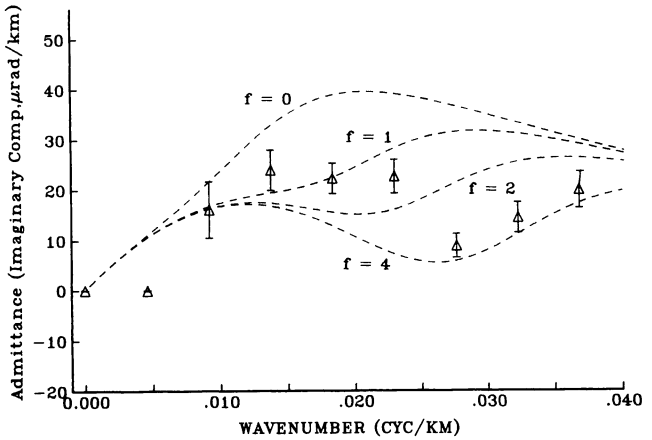

Fig. 12*f*. Admittances (imaginary component only) observed along the combination of legs A, B, and C. Dashed lines are imaginary theoretical admittances predicted by a model in which subseafloor and seafloor loads on 2-km-thick lithosphere are combined in the ratio f = 0, 1, 2, and 4.

z_l = 4, 6, and 9 km. Admittances in Figures 12*c*, 12*d*, and 12*e* are calculated for three load depths: z_l = 6, 9, and 14 km beneath the seafloor. Overall, it is not clear which model load depth is preferred by the observations; it appears that any model which includes a thin (~2 km) lithosphere loaded at roughly Moho depth (i.e., 6 km beneath the seafloor) should provide a fair agreement with admittances observed along zigs 1, 2, 3, and 6. Note that for a load depth z_l = 6 km, theoretical admittances take on negative imaginary, as opposed to positive imaginary, values at short wavelengths (λ < 40 km). In other words, predicted phases switch from $+\pi/2$ to $-\pi/2$. We have plotted this predicted phase switch in Figures 13*b*, 13*c*, and 13*e*. We do not attach too much significance to the rough agreement between predicted and observed phases in Figures 13*b*, 13*c*, and 13*e*. We do, however believe that the negative imaginary admittances are significant. They indicate that zones of buoyant, low-density material lie beneath the lineations most probably at Moho depths. Comparing bathymetric profiles (e.g., Figure 3*a*, southern part, and Figure 6*a*) with corresponding geoid profiles (Figures 3*b* and 6*b*), one can see short-wavelength (λ < 75 km) geoid lows that occur near the crests of lineations usually in association with the narrow, volcanic

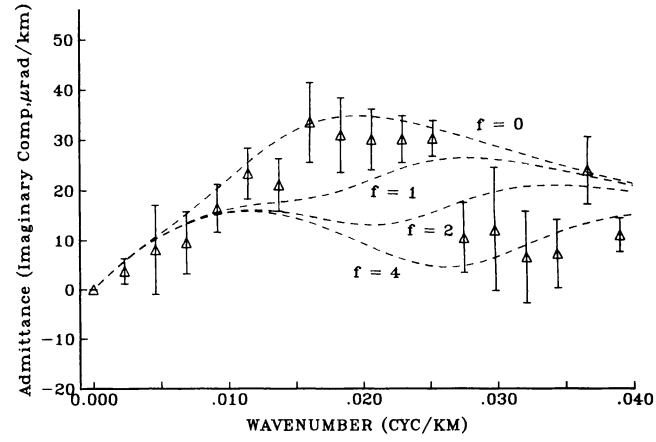

Fig. 12*g*. Admittances (imaginary component only) observed along zig 6 (same as Figure 12*a*). Dashed lines are theoretical admittances predicted by the same combined load model used in Figure 12*f*, except that ocean depth d = 5 km instead of 4 km.

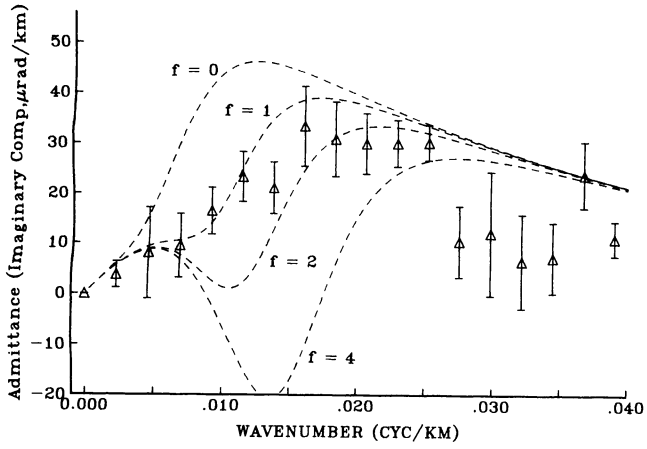

Fig. 12*h*. Admittances (imaginary component only) observed along zig 6 (same as Figures 12*a* and 12*g*). Dashed lines are theoretical admittances predicted by a model in which subseafloor and seafloor loads on 5-km-thick lithosphere are combined in the ratio $f = 0$, 1, 2, and 4.

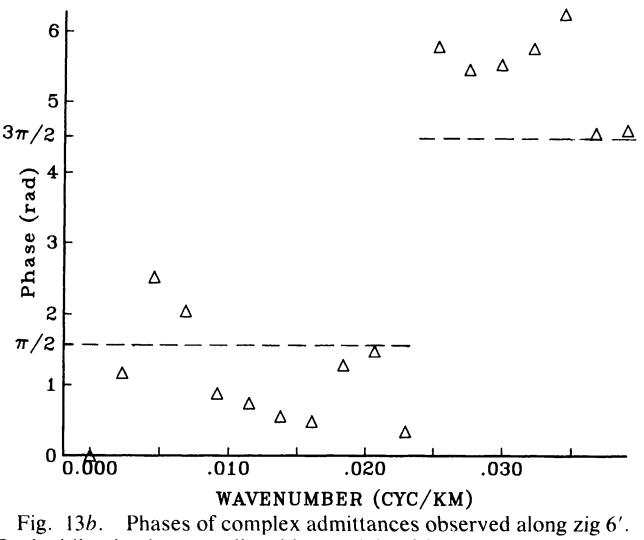

Fig. 13*b*. Phases of complex admittances observed along zig 6′. Dashed line is phase predicted by models of flexural compensation (T_e = 2 km) with loading beneath the seafloor at z_l = 6 km.

ridges. We feel that these geoid lows help produce the negative admittances.

Combined Loading: On and Beneath the Seafloor

Forsyth [1985] considered the problem of estimating average admittance when two different forms of lithospheric loading (top and bottom loading) are both operative. When the top and bottom loading are statistically independent processes, Forsyth's results yield the following expression for expected, combined admittance Z_d:

$$Z_d = \frac{\phi^2 Z_d^b + Z_d^t}{\phi^2 + 1} \tag{8a}$$

where

$$\phi = f\left[\frac{\rho_c - \rho_w}{\rho_m - \rho_c + Dk^4/g}\right] \tag{8b}$$

In equation (8*b*), f is the ratio of bottom load to top load, and in (8*a*), Z_d^b is admittance for bottom loading given by (7) and Z_d^t is admittance for top loading given by (6). Equation (8*a*) was used to compute the admittances shown in Figures 12*f*, 12*g*, and 12*h*. In evaluating (8*a*), we use the same values for parameters E, ν, ρ_m, ρ_c, ρ_w, and t which we used to evaluate (6) and (7) individually.

Theoretical admittances plotted as dashed lines in Figure 12*f* result from a 2-km-thick lithosphere loaded on top and bottom (z_l = 6 km) with load ratios f of 0, 1, 2, and 4. Ocean depth d is 4 km. Admittances observed along the combined legs A, B, and C are also plotted in Figure 12*f*, and they agree reasonably well with the theoretical admittances for load factors f ranging from 1 to 3. In other words, these observed admittances suggest that a combination of top and bottom loading is acting on a thin lithosphere and that the bottom loading is somewhat greater than the top. Note that the admittance observed at the longest finite wavelength, or lowest nonzero wave number, k = 0.0049 cycles/km (Figure 12*f*), is near zero and does not agree well with theoretical admittances. In fact, this admittance is not predicted by any

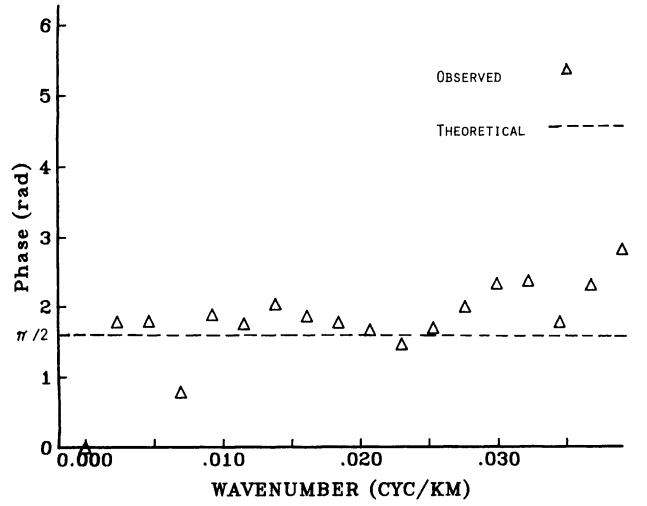

Fig. 13*a*. Phases of complex admittance observed along zig 6. Dashed line is phase predicted by models of flexural compensation with loading on the seafloor.

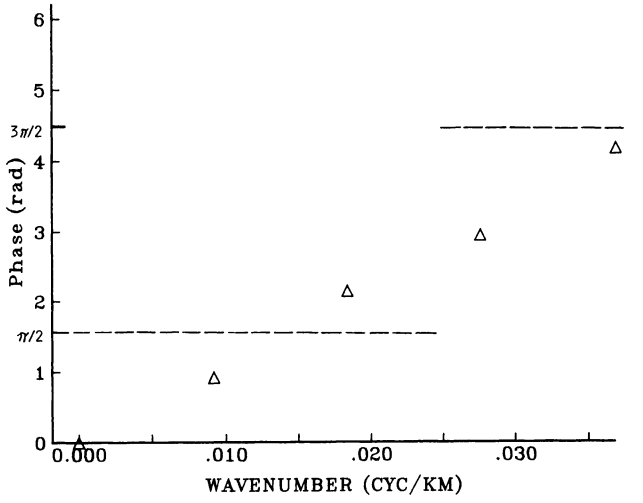

Fig. 13*c*. Phases of complex admittance observed along zig 1. Dashed line is phase predicted by models of flexural compensation with loading beneath the seafloor at z_l = 6 km.

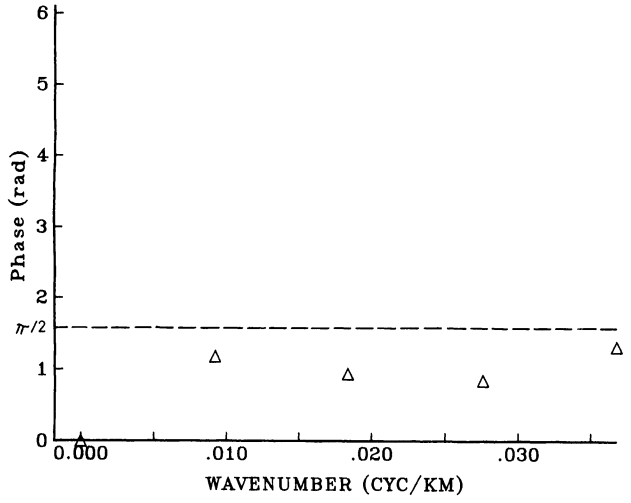

Fig. 13*d*. Phases of complex admittance observed along zig 2. Dashed line same as in Figure 13*c*, except $z_l > 9$ km.

reasonable model; its associated phase (see Figure 13*f*) is π, not $\pi/2$, and its associated coherence is also near zero. We can probably disregard this admittance.

In Figure 12*g*, we have plotted virtually the same theoretical admittances which were plotted in the preceding figure (Figure 12*f*). In this case we used a greater ocean depth of $d = 5$ km. Also shown in Figure 12*g* are the admittances observed along zig 6, replotted from Figure 12*a*. Once again, the model of combined bottom and top loading on a thin ($T_e = 2$ km) lithosphere predicts, reasonably well, the observed admittances.

It is noteworthy that a (combined loading) model which predicts, rather well, admittances observed over 5- to 10-m.y.-old cross-grain crust (legs A, B, and C) also does a good job of predicting admittances over the 40- to 50-m.y.-old crust (zig 6). How well will a similar model with a somewhat thicker lithosphere, $T_e = 5$ km as opposed 2 km, perform? In Figure 12*h*, we see that such a model successfully predicts longer-wavelength ($\lambda > 50$ km) admittances observed, once again, along zig 6. So, it appears that the operative lithospheric thickness may be as large as 5 km. However, this thicker

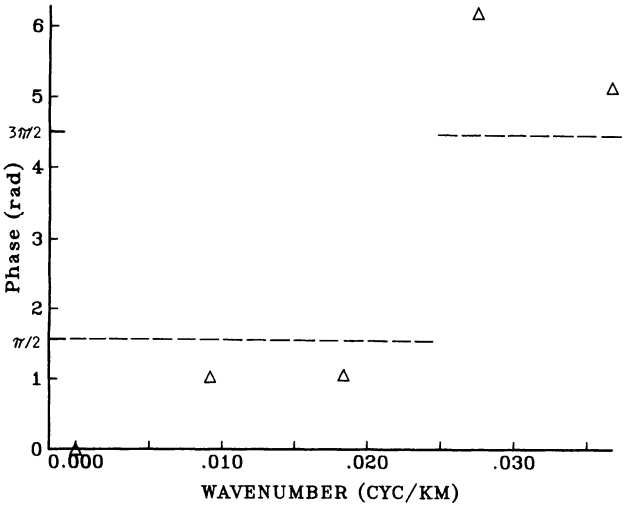

Fig. 13*e*. Phases of complex admittance observed along zig 3. Dashed line same as in Figure 13*c*.

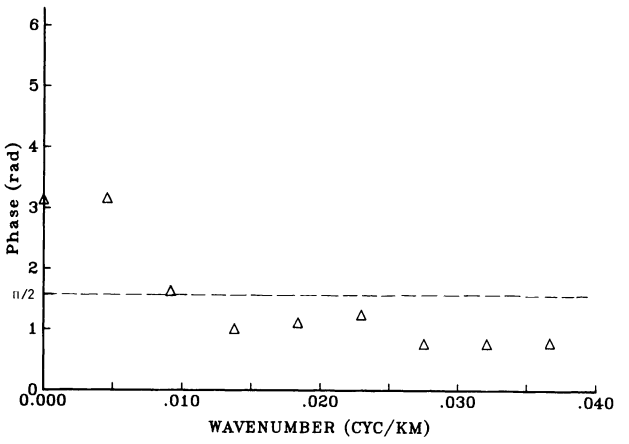

Fig. 13*f*. Phase of complex admittance observed along legs A, B, and C in combination. Dashed line is model-predicted phase.

lithosphere model can not explain the low admittances observed at wavelengths between 25 and 50 km.

Discussion

This is the first intensive study of relationships between gravity and bathymetry over the cross-grain lineations. We find no direct evidence for active small-scale mantle convection beneath the lineations. (We are not looking for convection on intermediate scales of several thousand kilometers proposed by *Watts et al.* [1985] and *Black and McAdoo* [1989].) More specifically, when we compare our observed admittances with those predicted by models of upper mantle convection [*Parsons and Daly*, 1983], we find little agreement. The models of *Parsons and Daly* [1983] predict, for any reasonable choice of convecting layer depth, admittances which, in the range $k' = 0.003$–0.01 cycle/km, are nearly equal to those of uncompensated topography, i.e., are much larger than our observed admittances. We can not, however, firmly conclude that these lineations are unrelated to thermal convection in the upper mantle. We are faced with a paradox: our study which spans crustal ages from 6 to 75 Ma indicates that these lineations are rooted at shallow, crustal depths and may result from tensional cracking of the lithosphere; on the other hand, these lineations trend parallel to the Hawaiian Chain thereby following the course of a hotspot embedded in the mantle beneath the Pacific plate. It is perhaps conceivable that these lineations might result from crustal/upper mantle density anomalies which are emplaced via small-scale convection at, or very near, the East Pacific Rise. This is basically the same proposition as that put forward by *Buck and Parmentier* [1986]. They suggested that the lineations were "frozen in." There exists, however, a problem with this hypothesis. If these lineations on older

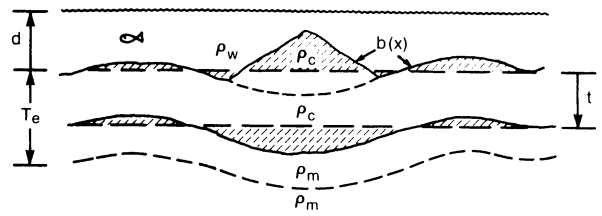

Fig. 14*a*. Flexural compensation model of loading on the seafloor.

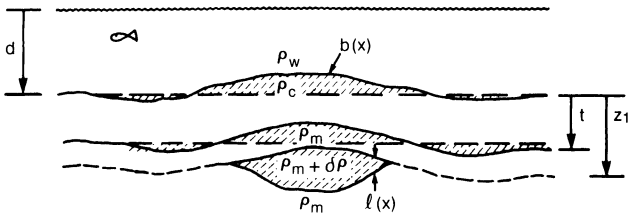

Fig. 14*b*. Flexural compensation model of loading beneath the seafloor. As drawn, $\delta\rho$ is negative, i.e., load at depth z_l is buoyant.

crust (age 50–70 Ma) were "frozen in" at or very near the East Pacific Rise, then their age would be roughly equal to the Emperor Seamounts. If this were true, these lineations ought to be aligned in the direction of past, not present, absolute motion, i.e., aligned parallel to the Emperor Chain. Clearly, more surface ship observations and analyses are needed to sort out these possibilities.

Our analysis has several limitations. Most obvious is the fact that we have ignored the sediments. However, it is very difficult to "backstrip" the sediments properly without some knowledge of the relative histories of sedimentation and lineation formation. Suppose that the sediments mostly predate lineations and sedimentary layers are conformable with basement topography, then our analysis is not affected by the sediments. If significant sedimentation occurred following lineation formation, the bathymetric signal would be attenuated and admittances would be amplified. If this is, indeed, the situation in our study area, then our observed admittances (already low admittances) are exaggerated and true admittances would be even smaller. A second limitation involves our use of one-dimensional admittance models. If our bathymetry and observed gravity are lineated transversely to our ship/satellite tracks, as they seem to be, this is not a problem. If we had highly detailed bathymetric observations of regions flanking the satellite passes, then we could assess whether our one-dimensional analysis is significantly corrupted by the effects of two-dimensional bathymetry.

Conclusions

We have analyzed, in the Fourier transform domain, relationships between Geosat gravity and coincident bathymetry over the cross-grain lineations. These lineations, which are located in the east central Pacific, have been attributed to small-scale convection in the upper mantle. We have analyzed lineations in crust which ranges in age from 6 to 75 Ma, and we find no evidence for such convection or dynamic compensation. Instead, we find the lineations to be superficial features that result, apparently, from a combination of subsurface and surface loads which are supported by a thin (2 km to perhaps 5 km) lithosphere. These subsurface loads are located roughly at Moho depths.

The nature of these loads is uncertain. We prefer to think that they resulted from tensional cracking and intrusion which may, in turn, have arisen due to intraplate thermal contraction or slab pull. It is also conceivable, but somewhat problematic, that these loads are delivered by small-scale convection very near the East Pacific Rise.

Acknowledgments. We thank the reviewers, in particular, Carl Bowin for helpful and thorough reviews. Maria Zuber read a preliminary version of this manuscript and made helpful suggestions. David T. Sandwell was supported by the NASA Geodynamics Program (NAG5-787).

References

Banks, R. J., R. L. Parker, and S. P. Huestis, Isostatic compensation on a continental scale: Local versus regional mechanism, *Geophys. J. R. Astron. Soc.*, *51*, 431–452, 1977.

Barrell, J., The strength of the Earth's crust, 8, Physical conditions controlling the nature of the lithosphere and asthenosphere, *J. Geol.*, *22*, 425–443, 1914.

Black, M. T., and D. C. McAdoo, Spectral analysis of marine geoid heights and ocean depths: Constraints on models of lithospheric, and sublithospheric processes, *Mar. Geophys. Res.*, in press, 1989.

Buck, W. R., and E. M. Parmentier, Convection beneath young oceanic lithosphere: Implications for thermal structure and gravity, *J. Geophys. Res.*, *91*, 1961–1974, 1986.

Cheney, R. E., B. C. Douglas, R. W. Agreen, L. L. Miller, D. L. Porter, and N. S. Doyle, Geosat altimeter geophysical data record user handbook, *NOAA Tech. Memo.*, *NOS NGS-46*, 1987.

Chapman, M. E., Techniques for interpretation of geoid anomalies, *J. Geophys. Res.*, *84*, 3793–3802, 1979.

Dorman, L. M., and B. T. R. Lewis, Experimental isostasy, 1, Theory of the determination of the Earth's isostatic response to a concentrated load, *J. Geophys. Res.*, *75*, 3357–3365, 1970.

Forsyth, D. W., Subsurface loading and estimates of the flexural rigidity of continental lithosphere, *J. Geophys. Res.*, *90*, 12,623–12,632, 1985.

Gunn, R., A quantitative evaluation of the influence of the lithosphere on the anomalies of gravity, *J. Franklin Inst.*, *236*, 373–396, 1943.

Haxby, W. F., Gravity field of the world's oceans, map from Seasat data, Natl. Geophys. Data Cent., NOAA, Boulder, Colo., 1987.

Haxby, W. F., and J. K. Weissel, Evidence of small-scale convection from Seasat altimeter data, *J. Geophys. Res.*, *91*, 3507–3520, 1986.

Lin, J., and E. M. Parmentier, Surface topography due to convection in variable viscosity fluid: Application to short wavelength gravity anomalies in the central Pacific Ocean, *Geophys. Res. Lett.*, *12*, 357–360, 1985.

McKenzie, D., and C. Bowin, The relationship between bathymetry in the Atlantic Ocean, *J. Geophys. Res.*, *81*, 1903–1915, 1976.

McNutt, M. K., Influence of plate subduction on isostatic compensation in northern California, *Tectonics*, *2*, 399–415, 1983.

Munk, W. H., and D. E. Cartwright, Tidal spectroscopy and prediction, *Philos. Trans. R. Soc. London, Ser. A*, *259*, 533–581, 1966.

Parsons, B., and S. Daly, The relationship between surface topography, gravity anomalies, and temperature structure of convection, *J. Geophys. Res.*, *88*, 1129–1144, 1983.

Richter, F. M., and B. Parsons, On the interactions of two scales of convection in the mantle, *J. Geophys. Res.*, *80*, 2529–2541, 1975.

Sandwell, D. T., and D. C. McAdoo, Marine gravity of the southern ocean and Antarctic margin from Geosat, *J. Geophys. Res.*, *93*, 10,389–10,396, 1988.

Vening Meinesz, S. A., Tables fondamentals pour la reduction isostatique regionale, *Bull. Geod.*, *63*, 711–776, 1939.

Walcott, R. I., Lithospheric flexure, analysis of gravity anomalies, and the propagation of seamount chains, in *The Geophysics of the Pacific Ocean Basin and Its Margin, Geophys. Monogr. Ser.*, vol. 19, edited by G. H. Sutton, M. H. Manghnani, and R. Moberly, pp. 431–438, AGU, Washington, D. C., 1976.

Watts, A. B., On geoid heights derived from Geos 3 altimeter data along the Hawaiian-Emperor seamount chain, *J. Geophys. Res.*, *84*, 3817–3826, 1978.

Watts, A. B., D. P. McKenzie, B. E. Parsons, and M. Roufosse, The relationship between gravity and bathymetry in the Pacific Ocean, *Geophys. J. R. Astron. Soc.*, *83*, 263–298, 1985.

Winterer, E. L., and D. T. Sandwell, Evidence from en echelon crossgrain ridges for tensional cracks in the Pacific plate, *Nature*, *329*, 534–537, 1987.

D. C. McAdoo, National Geodetic Survey, Charting and Geodetic Services, National Ocean Service, NOAA, Rockville, MD 20852.

D. T. Sandwell, Center for Space Research, University of Texas at Austin, Austin, TX 78712.

(Received May 24, 1988;
revised January 6, 1989;
accepted March 27, 1989.)